Antarctic Science 3 (2): 187–195 (1991)

Numerical modelling of ice shelf dynamics

JÜRGEN DETERMANN

Alfred Wegener Institute for Polar and Marine Research, Columbusstrasse, D-2850 Bremerhaven, Germany

Abstract: By considering the basic stress equations for a unit volume of ice, a set of differential equations describing ice shelf flow is derived. In view of the lack of basal shear stresses at the bottom of ice shelf a model simulation which is restricted to the horizontal dimensions will not imply substantial errors. The model is applied to the Filchner-Ronne Ice Shelf, Antarctica, and model equations are solved in terms of finite differences on a 10 x 10 km grid. Present ice thickness data and boundary conditions, i.e. the balance velocities at the grounding line and strain rates at the ice front are entered as input. Using a non-linear Glen-type flow law (n=3) and a constant depth-averaged flow law parameter, representing an ice temperature of -17°C, a convincing velocity field is derived as a solution of the model equations. The model takes into account restrained flow across ice rumples where sufficient field data are available. A diagnostic run reproducing present velocity magnitudes is followed by two prognostic runs, each representing 2000 years of simulation. Transient ice thickness changes are obtained from solving the mass conservation equation. Two different assumptions concerning basal melting rates demonstrate its importance to ice shelf dynamics. Assumptions are: a) no basal melting, b) basal melting rates (-2m a^{-1} to +3m a^{-1}) as derived from model results and geophysical field data.

Received 2 November 1989, accepted 26 December 1990

Key words: basal melting, Filchner-Ronne Ice Shelf, finite-differences, time-dependent simulations.

Introduction

Ice shelves form when ice masses flowing out from the Antarctic ice sheet begin to float in the ocean. This happens at the grounding line, which is the landward margin of an ice shelf. As early as 1957, Weertman (1957) investigated the creep deformation of floating ice shelves. Budd (1966) and Thomas (1973) presented extended theories which all dealt with ice thickness profiles in relation to strain rates. Unlike Sanderson (1979), who stated that most ice shelves surrounding Antarctica are not in equilibrium, Van der Veen (1986) determined from time-dependent simulations that ice shelves are always close to steady state.

Recently, a number of papers dealing with ice shelf modelling have been published. MacAyeal & Thomas (1982) used the finite-element method (FE) to simulate the dynamics of the Ross Ice Shelf, and Lange & MacAyeal (1986) have done the same to describe the movement of Filchner-Ronne Ice Shelf (FRIS). FE-simulations are known to be the most accurate method for numerical solutions, whereas the advantages of finite-differences methods (FD) are simplicity and easy handling of variable grid boundaries, an aspect that might be important when dealing with transient changes in the extent of the ice shelf.

Following a derivation of Herterich (1987) for the transition zone between the ice sheet and ice shelf a model for two-dimensional horizontal ice shelf motion will be presented. The model equations are solved by means of the finite-differences method using balance fluxes at the grounding line and strain rates at the ice front as boundary conditions. If flow law parameters are determined, the ice thickness distribution is the important quantity for yielding flow velocities of the entire ice shelf. In order to get information about transient ice thickness changes, the velocity field enters into the mass conservation equation which comprises flux divergence and accumulation minus melting. Arising from this, the effect of laterally varying mass balances on the steady-state ice shelf profile are studied.

Known as the biggest ice shelf in the world by volume (Swithinbank 1988), FRIS makes an important contribution to the drainage of Antarctica. Freezing and melting underneath the ice shelf contribute to the mass budget, as does the influx from ice streams and surface accumulation. Melting, observed beneath the ice front by Behrendt (1970), governs the formation of cold ice shelf water. Basal freezing, on the other hand is required to explain the existence of a strongly reflecting internal radio-echo horizon in the central part of FRIS (Thyssen 1988). In this paper the term 'freezing' refers to bottom accretion due to heat conduction as well as to the release of ice crystals that grow in the water column underneath the ice shelf. Although it has not been conclusively proved, the basal ice is referred to as "saline" ice. Basal accumulation rates are deduced from the continuity equation which is applied to describe the present shape of the basal ice layer.

Model equations

The following derivation, which will lead to a set of differential equations describing two-dimensional ice shelf flow, is based on substantial theoretical work undertaken by Weertman (1957), Budd (1966), Thomas (1973), Sanderson (1979), Van der Veen (1986) and others. In order to describe the flow in a vertical plane across the ice sheet/ice shelf junction, Herterich (1987) proposed a similar method. By considering force balance for a unit volume of ice, Newton's second law yields the following set of basic stress equations (Jaeger 1969):

$$\frac{\partial \tau_{xx}}{\partial x} + \frac{\partial \tau_{xy}}{\partial y} + \frac{\partial \tau_{xz}}{\partial z} = 0, \tag{1}$$

$$\frac{\partial \tau_{xy}}{\partial x} + \frac{\partial \tau_{yy}}{\partial y} + \frac{\partial \tau_{yz}}{\partial z} = 0, \tag{2}$$

$$\frac{\partial \tau_{xz}}{\partial x} + \frac{\partial \tau_{yz}}{\partial y} + \frac{\partial \tau_{zz}}{\partial z} = -\rho_i g \tag{3}$$

where τ_{ij} are the components of the stress tensor T, ρ_i the ice density and g the acceleration due to gravity which is negative due to the chosen coordinate system. X and y are the horizontal coordinates, with x pointing downstream, and z, the vertical coordinate being positive upwards and zero at sea level. Under ice shelf conditions (no vertical shear) one can neglect $\partial\tau_{xz}/\partial x$ and $\partial\tau_{yz}/\partial y$ in equation (3). Vertical integration then yields:

$$\tau_{zz}(z) = -\rho_i g(z_s - z). \tag{4}$$

The flow properties of ice are often held to be independent of the hydrostatic pressure P, which is defined as

$$P = \tfrac{1}{3}(\tau_{xx} + \tau_{yy} + \tau_{zz}).$$

Subtraction of P from T according to:

$$\tau'_{ij} = \tau_{ij} - \delta_{ij} P$$

yields the elements of the stress deviator τ'. In particular,

$$\tau'_{xx} = \tau_{xx} - \tfrac{1}{3}(\tau_{xx} + \tau_{yy} + \tau_{zz}), \tag{5}$$

$$\tau'_{yy} = \tau_{yy} - \tfrac{1}{3}(\tau_{xx} + \tau_{yy} + \tau_{zz}) \tag{6}$$

are the longitudinal stress deviators. A combination of (5) and (6) gives:

$$2\tau'_{xx} + \tau'_{yy} = \tau_{xx} - \tau_{zz} \tag{7}$$

and

$$2\tau'_{yy} + \tau'_{xx} = \tau_{yy} - \tau_{zz} \tag{8}$$

which, inserted into (1) and (2) yield:

$$\frac{\partial}{\partial x}(2\tau'_{xx} + \tau'_{yy} + \tau_{zz}) + \frac{\partial \tau_{xy}}{\partial y} + \frac{\partial \tau_{xz}}{\partial z} = 0, \tag{9}$$

$$\frac{\partial}{\partial y}(2\tau'_{yy} + \tau'_{xx} + \tau_{zz}) + \frac{\partial \tau_{xy}}{\partial x} + \frac{\partial \tau_{yz}}{\partial z} = 0. \tag{10}$$

According to (4), the normal stress deviator gradients depend on the ice surface elevation gradients $\partial z_s/\partial x$ which are related to the ice thickness H according to the buoyancy condition:

$$z_s = \left(1 - \frac{\rho_i}{\rho_w}\right) H$$

where ρ_i and ρ_w are the densities of ice and sea water, respectively. Substituting the horizontal gradients of (4) into (9) and (10), the following set of differential equations holds:

$$-\rho_i g \frac{\partial z_s}{\partial x} + 2\frac{\partial \tau'_{xx}}{\partial x} + \frac{\partial \tau'_{yy}}{\partial x} + \frac{\partial \tau_{xy}}{\partial y} + \frac{\partial \tau_{xz}}{\partial z} = 0, \tag{11a}$$

$$-\rho_i g \frac{\partial z_s}{\partial y} + 2\frac{\partial \tau'_{yy}}{\partial y} + \frac{\partial \tau'_{xx}}{\partial y} + \frac{\partial \tau_{xy}}{\partial x} + \frac{\partial \tau_{yz}}{\partial z} = 0. \tag{11b}$$

As it is not possible to measure directly stresses in field experiments (Hutter 1983), equation (11) has to be transformed in a way that makes it more suitable to assimilate field data. This can be done by introducing a flow law for ice such as Glen's law (1955), which relates strain rates and stresses according to:

$$\dot{\epsilon}_{ij} = A\tau^{n-1}\tau'_{ij}. \tag{12}$$

Here ε_{ij} is a strain tensor element, A a temperature-dependent flow law parameter and τ the effective stress, which is defined as the second invariant of the stress tensor.

$$2\tau^2 = \tau_{xx}^2 + \tau_{yy}^2 + \tau_{zz}^2 + 2(\tau_{xy}^2 + \tau_{xz}^2 + \tau_{yz}^2). \tag{13}$$

Usual glaciological practice is to set the exponent n equal to three (Paterson 1981). The effective strain rate $\dot{\epsilon}$ is given by:

$$\dot{\epsilon} = A\tau^n, \tag{14}$$

which can be combined with equation (12) to give

$$\tau'_{ij} = \dot{\epsilon}_{ij} A^{-\frac{1}{n}} \dot{\epsilon}^{\frac{1}{n}-1}. \tag{15}$$

According to the principles of continuum mechanics one can express strain rates in terms of velocity gradients as:

$$\dot{\epsilon}_{ij} = \frac{1}{2}\left(\frac{\partial u_i}{\partial x_j} + \frac{\partial u_j}{\partial x_i}\right) \tag{16}$$

https://doi.org/10.1017/S0954102091000226 Published online by Cambridge University Press

so that $\dot{\varepsilon}^{\frac{1}{n}-1}$ replaced by f, is equal to:

$$f = \left\{\frac{1}{2}\left[\left(\frac{\partial u}{\partial x}\right)^2 + \left(\frac{\partial v}{\partial y}\right)^2 + \left(\frac{\partial w}{\partial z}\right)^2 + \frac{1}{2}\left(\frac{\partial u}{\partial y} + \frac{\partial v}{\partial x}\right)^2 + \frac{1}{2}\left(\frac{\partial u}{\partial z} + \frac{\partial w}{\partial x}\right)^2 + \frac{1}{2}\left(\frac{\partial v}{\partial z} + \frac{\partial w}{\partial y}\right)^2\right]\right\}^{\frac{\frac{1}{n}-1}{2}}. \quad (17)$$

Then, finally inserting (15) into (11), the following set of equations, which describe the flow of an ice shelf, is obtained.

$$-\gamma\frac{\partial z_s}{\partial x} + 2\frac{\partial}{\partial x}\left(f\frac{\partial u}{\partial x}\right) + \frac{\partial}{\partial x}\left(f\frac{\partial v}{\partial y}\right) + \frac{1}{2}\frac{\partial}{\partial y}\left[f\left(\frac{\partial u}{\partial y} + \frac{\partial v}{\partial x}\right)\right] + \frac{1}{2}\frac{\partial}{\partial z}\left[f\left(\frac{\partial u}{\partial z} + \frac{\partial w}{\partial x}\right)\right] = 0, \quad (18a)$$

$$-\gamma\frac{\partial z_s}{\partial y} + 2\frac{\partial}{\partial y}\left(f\frac{\partial v}{\partial y}\right) + \frac{\partial}{\partial y}\left(f\frac{\partial u}{\partial x}\right) + \frac{1}{2}\frac{\partial}{\partial x}\left[f\left(\frac{\partial u}{\partial y} + \frac{\partial v}{\partial x}\right)\right] + \frac{1}{2}\frac{\partial}{\partial z}\left[f\left(\frac{\partial v}{\partial z} + \frac{\partial w}{\partial y}\right)\right] = 0, \quad (18b)$$

with

$$\gamma = \rho_i g A^{\frac{1}{n}}.$$

Since there is a lack of shear stress at the ice shelf bottom, $\partial u/\partial z$ and $\partial v/\partial z$ are negligible (Sanderson & Doake 1979). Furthermore, the horizontal gradients of the vertical velocity component w are assumed to be small compared with those of u and v, which makes (18) even simpler (typical values are: $\partial u/\partial x = 10^{-3}$, $\partial w/\partial x < 10^{-4}$). The remnant equations (19) contain quantities which are, except for A and n, available from field measurements.

$$-\gamma\frac{\partial z_s}{\partial x} + 2\frac{\partial}{\partial x}\left(f\frac{\partial u}{\partial x}\right) + \frac{\partial}{\partial x}\left(f\frac{\partial v}{\partial y}\right) + \frac{1}{2}\frac{\partial}{\partial y}\left[f\left(\frac{\partial u}{\partial y} + \frac{\partial v}{\partial x}\right)\right] = 0, \quad (19a)$$

$$-\gamma\frac{\partial z_s}{\partial y} + 2\frac{\partial}{\partial y}\left(f\frac{\partial v}{\partial y}\right) + \frac{\partial}{\partial y}\left(f\frac{\partial u}{\partial x}\right) + \frac{1}{2}\frac{\partial}{\partial x}\left[f\left(\frac{\partial u}{\partial y} + \frac{\partial v}{\partial x}\right)\right] = 0. \quad (19b)$$

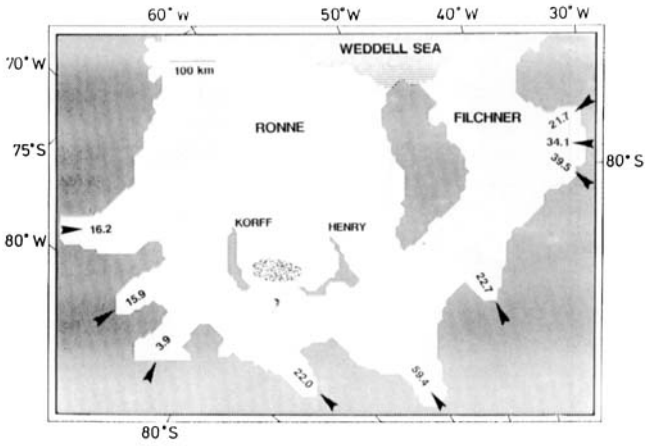

Fig. 1. Filchner-Ronne Ice shelf (FRIS), Antarctica. Nine ice streams and outlet glaciers drain into the ice shelf. Balance fluxes magnitudes are given in $km^3\ a^{-1}$ (Mclntyre 1986). They determine the flow velocities at the grounding line. The shaded area between Henry and Korff ice rises indicates the location of Doake Ice Rumples (DIR).

where

$$f = \left\{\left(\frac{\partial u}{\partial x}\right)^2 + \left(\frac{\partial v}{\partial y}\right)^2 + \left(\frac{\partial u}{\partial x}\right)\left(\frac{\partial v}{\partial y}\right) + \frac{1}{4}\left(\frac{\partial u}{\partial y} + \frac{\partial v}{\partial x}\right)^2\right\}^{\frac{1-n}{2n}} \quad (20)$$

using continuity:

$$\dot{\epsilon}_{xx} + \dot{\epsilon}_{yy} + \dot{\epsilon}_{zz} = 0.$$

The solution of (19a and b) which represents the velocity field for the entire ice shelf can be accomplished when boundary conditions have been specified below.

Experiments

Three runs labelled A, B and C are performed in this section. A gives the velocity field to the present-day ice thickness distribution and, in runs B and C the time-dependent mass balance equation is used to demonstrate 2000 years of future ice shelf evolution.

A: Velocity field - diagnostic simulation

The first aim in developing this model is to describe and reproduce the present-day flow velocities for FRIS. To achieve these as solutions of the model equations (19) one must start with the determination of the ice thickness distribution for the entire ice shelf. Thickness data (Fig. 2a) are the same as those used for FE-simulations by Lange & MacAyeal (1986). Equation (19) is a boundary problem of the mixed Dirichlet - Neuman type, with a rigid condition at the grounding line and an open boundary on the seaward side. Boundary conditions are fixed velocities at the grounding

https://doi.org/10.1017/S0954102091000226 Published online by Cambridge University Press

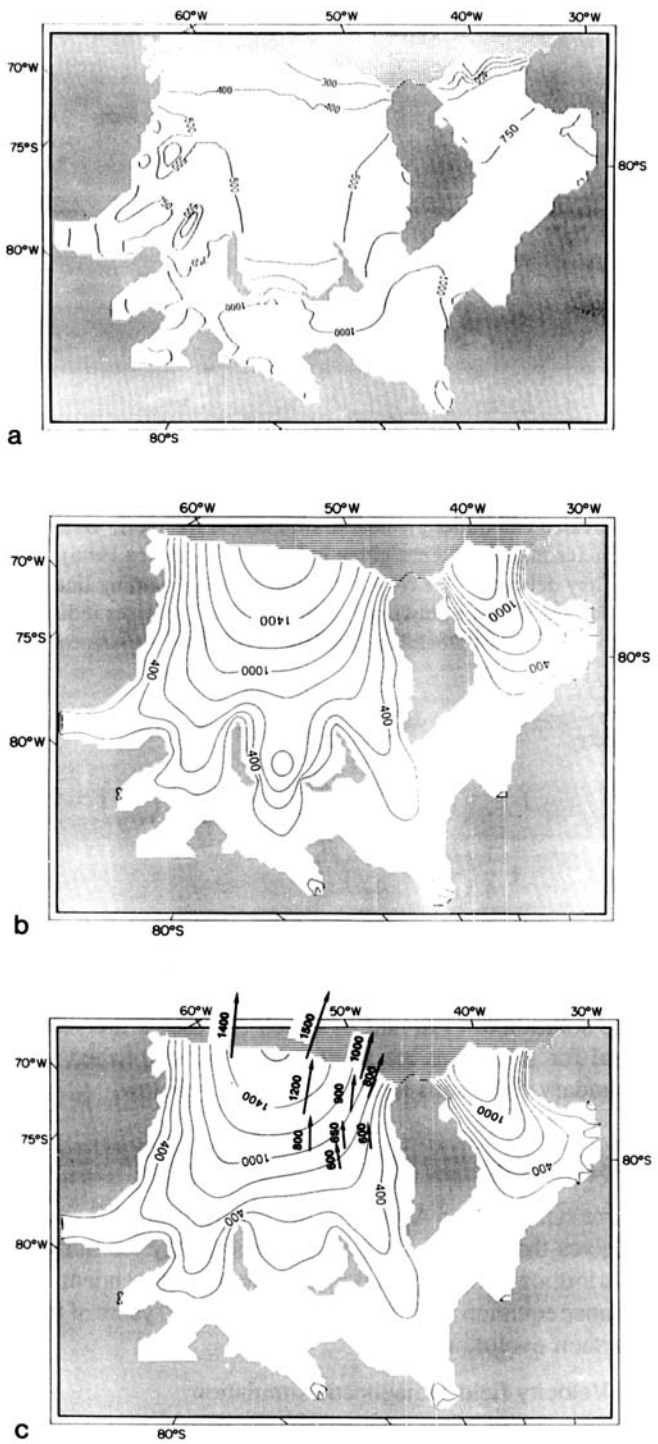

Fig. 2. a. Ice thickness distribution, already corrected for the basal layer of "saline" ice in the central part.

b. Diagnostic run on the basis of the actual ice thickness distribution; the restraint which is exerted by Doake Ice Rumples (DIR) is not taken into account. Contour lines of simulated velocities are given in m a^{-1}. One can state a general consistency with the results from Lange & MacAyeal (1986), also for the ice rumples area where simulated velocities exceed observations by one order of magnitude.

c. Diagnostic run (A), including the restraint by DIR. The velocity magnitudes are improved for the ice rumples area. Downstream of Henry and Korff ice rises they are slightly lower compared with the previous run. Contour lines are given in comparison with measurements by Kock & Wiegand (1986).

line and the longitudinal strain rates at the ice front. McIntyre (1986) specified the ice inflow at the landward ice shelf margins in terms of balance fluxes (Fig. 1). These fluxes determine locally the velocities of nine ice streams and outlet mountain glaciers, whereas the ice is assumed to be stagnant elsewhere at the grounding line. Stagnant ice is also assumed for the margins of ice rises which are located inside the ice shelf area.

At the ice front, where the influence of sidewall restraints vanishes, an equation of Thomas (1973) applies, giving longitudinal strain rates in relation to ice thickness, density and the flow law parameter.

$$\dot{\epsilon}_{xx} = 3^{-\frac{n+1}{2}} A \cdot \left(\frac{\left(1 - \frac{\rho_i}{\rho_w}\right) \rho_i g H}{2} \right)^n . \qquad (21)$$

Both ice density and the flow law parameter are entered as vertically averaged quantities; this might magnify the strain rates by as much as threefold (Weertman 1957) and thus must be taken into consideration. Assuming an almost constant firn layer thickness for the entire ice shelf, the depth-averaged ice density ρ_i varies laterally depending on H. A relation which can be derived from Thyssen (1988) for FRIS:

$$\rho_i = 911 - \frac{13800}{H}$$

seems to express density variations sufficiently. Sea-water density ρ_w is taken to be 1027 kg m^{-3}.

After having expressed (19) in terms of finite differences, an explicit relaxation method yields the solution iteratively. After 5000 iterations the solution seems to be about 5–10% within asymptotic state (see Appendix).

The flow law parameter A is left as a free parameter which means that its magnitude solely governs the solution and determines the velocity field. Taking A to be 2.5 x 10^{-16} kPa^3 s^{-1}, which corresponds to a temperature of about -17 °C, a solution which agrees with the results derived by Lange & MacAyeal (1986) is obtained (Fig. 2b).

There is one location at FRIS where the model obviously fails. For the region between Henry and Korff ice rises the model yields velocities which exceed observations by one order of magnitude (Smith 1986). When looking closer at the problem, one recognizes that this feature is linked to local ice shelf grounding at Doake Ice Rumples (DIR). At

https://doi.org/10.1017/S0954102091000226 Published online by Cambridge University Press

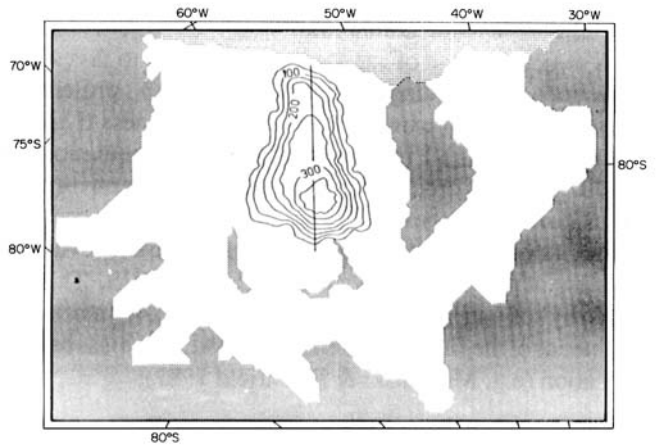

Fig. 3. FRIS basal-layer ice thickness: H_b given in m, as derived from isostatic anomalies (after Thyssen 1988)

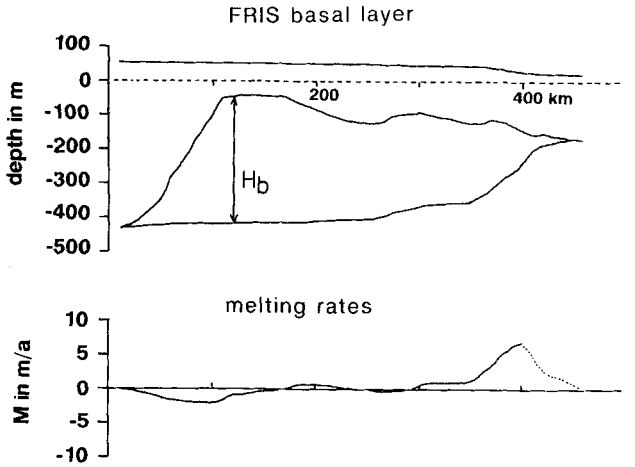

Fig. 4. FRIS ice thickness profile across the basal layer. Bottom melting rates according to equation (23) — negative values denote bottom freezing. Decreasing melting rates near the ice front (stippled line) arise from failure of (23) due to $H_b = 0$.

this location, a large downstream ice thickness gradient (Smith 1986) implies increasing flow velocities if floating conditions are assumed as in the model. However, because of grounding the flow becomes a combination of longitudinal stretching, shearing and basal sliding.

Unlike ice rises which have their own flow regime, ice flow across ice rumples is dependent on that of the ice shelf. Although in the past several attempts were undertaken to describe the behaviour of sliding ice streams and mountain glaciers (e.g. Budd *et al.* 1979, Bindschadler 1983, MacAyeal 1989), the physics of sliding is still poorly understood. MacAyeal (1989) investigated the role of basal drag exerted by a viscous layer of sediments on the flow of Ice Stream B, Antarctica. Thereafter, basal drag acts as a horizontal body force opposing the driving forces, but without causing substantial vertical shear. Assuming that basal drag acts in a similar way on DIR a practical attempt, rather than a physical one to improve the model, will be performed. Instead of evaluating restraining forces, driving forces caused by ice thickness gradients ($\partial H/\partial x$, $\partial H/\partial y$) are reduced in relation to the ice rumples height.

According to Swithinbank (1986) no known ice rumples rise more than z_0=30 m above ice shelf surface level. Taking this value as a threshold to discriminate between an ice rumple and an ice rise, one can apply a linear approach in order to adjust the flow across ice rumples. Surveying on a profile over Doake Ice Rumples by Smith (1986) yielded data concerning height above buoyancy z* (or height above ice shelf surface level) which are used to multiply ($\partial H/\partial x$, $\partial H/\partial y$) by a weighting factor r which is defined as:

$$r = \left(1 - \frac{z^*}{z_0}\right) \ldots z^* \leq z_0. \qquad (22)$$

Ice thickness gradients which govern ice shelf flow, are reduced to zero if z* equals z_0. In fact, this is an ice rise

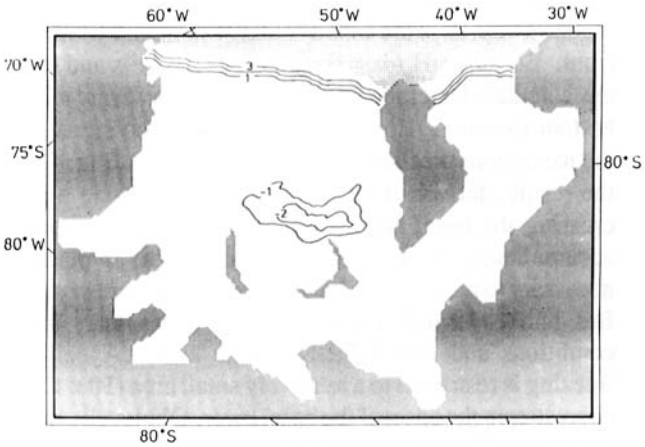

Fig 5. FRIS bottom melting rates, which are adopted in run C. Bottom accumulation rates in excess of 2 m a^{-1} occur in an area approx. 50 x 120 km downstream of Henry and Korff ice rises.

condition, whereas z*=0 implies pure ice shelf flow. In-between, ice rumples with $0 < z^* < z_0$ act as a brake by reducing the effectivity of ice thickness gradients. Running the model again now yields improved velocity magnitudes over DIR (Fig. 2c). With the exception of the area downstream of DIR where velocities decrease slightly, the flow remains mainly unchanged compared with the initial run. The solution is in good agreement with velocities observed by Kock & Wiegand (1986).

Surface and bottom mass balances

Surface accumulation and bottom freezing or melting contribute to the ice shelf dynamics as well as does the ice stream

https://doi.org/10.1017/S0954102091000226 Published online by Cambridge University Press

discharge. Surface mass balances have been observed from field measurements, whereas mass balances at the bottom have to be derived indirectly.

The central part of FRIS bears a thick layer of "saline ice" underneath an internal radio-echo reflecting horizon (Engelhardt & Determann 1987, Thyssen 1988). Isostatic anomalies published by Thyssen (1988) express the thickness H_b of this basal ice, which is assumed to be released from the ocean underneath (Fig. 3). By assuming mass conservation and a steady state ice shelf, the application of the continuity equation for mass on the formation of the basal layer, is suggested. Freezing or bottom accretion leads to an increase of H_b downstream when thinning due to spreading is small. Going further, melting plus spreading reduce H_b on approaching the ice front. In this sense, entering flow velocities from the diagnostic run and basal layer thicknesses into the continuity equation, yields bottom accumulation rates *m* according to:

$$m = -\frac{\partial}{\partial x}(H_b.u) - \frac{\partial}{\partial y}(H_b.v). \qquad (23)$$

This equation only holds if the basal ice has not completely melted away, as is the case about 30 km inland from the ice front. Because $\partial H_b/\partial x = 0$, equation (23) fails and reduces the calculated melting rates drastically or even indicates bottom freezing. However, clear radio-echo signals from the ice bottom preclude freezing at this place. Fig. 4 shows the results derived from (23) when going along a profile crossing the basal layer. Apparently, high rates of basal accumulation which exceed a rate of 2 m a^{-1} in places, are necessary to preserve the basal ice layer in its present extent. But unlike former assumptions of widespread freezing conditions underneath FRIS (Lange & MacAyeal 1988), freezing is restricted to a relatively small area (50 x 120 km) downstream the onset of the basal layer. Obviously, freezing rates of such a high magnitude can not be caused by heat conduction through the ice shelf/ocean boundary (Robin 1979). This strongly favours evidence for a mechanism like the 'ice pump' (Lewis & Perkin 1986), which redistributes ice masses from deeper to shallower water depths (Robin 1979).

Kohnen (1982) stated melting rates to be of the order of 3 m/a for the Ronne Ice Shelf. According to Behrendt (1970), melting rates for the Filchner Ice Shelf are greater than 3 m a^{-1}. Considering this, a melting rate of 3 m a^{-1} for the ice front region (< 50 km inland) seems to be reliable. Fig. 5 gives an overview of melting rates which can be adopted to time-dependent simulations. These are different from the 'steady state' melting rates (MacAyeal & Thomas 1986) which, at the grounding line may be influenced by inappropriately set boundary conditions. As the name implies, they maintain ice thicknesses in the present configuration. But this is in contrast to the objective of investigating transient ice shelf dynamics.

B and C:Transient changes of velocity and thickness distribution — time-dependent simulations.

A major purpose of ice shelf modelling is to investigate questions concerning stability based on present-day observations. For example, how do ice thickness H and the velocity field (u,v) react to changes in accumulation and melting rate? In order to demonstrate the long-term response to transient changes in accumulation, a time-dependent simulation, representing 2000 years of future evolution starting at present state, was conducted for FRIS. This was done by solving the mass balance equation (24) numerically by means of the finite-differences method. The mass balance equation (e.g. Muszinski & Birchfield 1987):

$$\frac{\partial H}{\partial t} = -\frac{\partial}{\partial x}(H.u) - \frac{\partial}{\partial y}(H.v) + a - m \qquad (24)$$

can be solved as soon as a diagnostic run has been completed. Here *t* stands for time, *a* for surface accumulation and *m* for bottom accumulation (m < 0) or melting. The mass balance equation requires ice incompressibility, and $\partial H/\partial t = 0$ would imply a steady state ice shelf, where the flux divergence and the accumulation rates cancel out.

In fact, the ice shelf imbalance ($\partial H/\partial t$) is not zero in the beginning of a simulation. H will decrease or increase locally and thus new ice thickness gradients arise, implying a new velocity field. A time step of 0.5 years is appropriate for accomplishing fast progress for the new steady state. Due to a lack of accurate data of bottom topography near the grounding line, a temporal change of the ice shelf extent is not considered in the present study. Nevertheless, one can learn where the ice shelf boundaries will tend to move. Two model runs with different assumptions on basal melting rates *m* were conducted. In run B, *m* was taken to be zero all over the ice shelf, whereas in run C, the melting rates from Fig. 5 were adopted. In both cases, the surface accumulation rates of about 0.2–0.4 m a^{-1} of ice equivalent from a compilation of Giovinetto & Bull (1987 p. 49) are entered. The flow law parameter A is kept constant for the time-dependent runs. Compared with the diagnostic run A, the dynamics of FRIS underwent remarkable changes in B and C. Figs. 6a & b show the new steady state for absence of basal melting. The central part of the ice shelf thinned slightly, probably as a result of restrained flow across DIR. The result would be even more drastic if the ice rumples completely blocked the ice flow. This was already mentioned in connection with the creation of the region of thin ice, detected by radio-echo soundings. Water masses ascending downstream could then release saline ice to form the basal layer (Lange & MacAyeal 1988). Simultaneously, ice thicknesses at the grounding line and at the ice front would increase by more than 200 m in places. In general, ice thickness gradients will tend to become smaller. The new shape corresponds to the new velocities in a way that mass conservation holds. Because of larger thicknesses at the grounding line, ice streams now

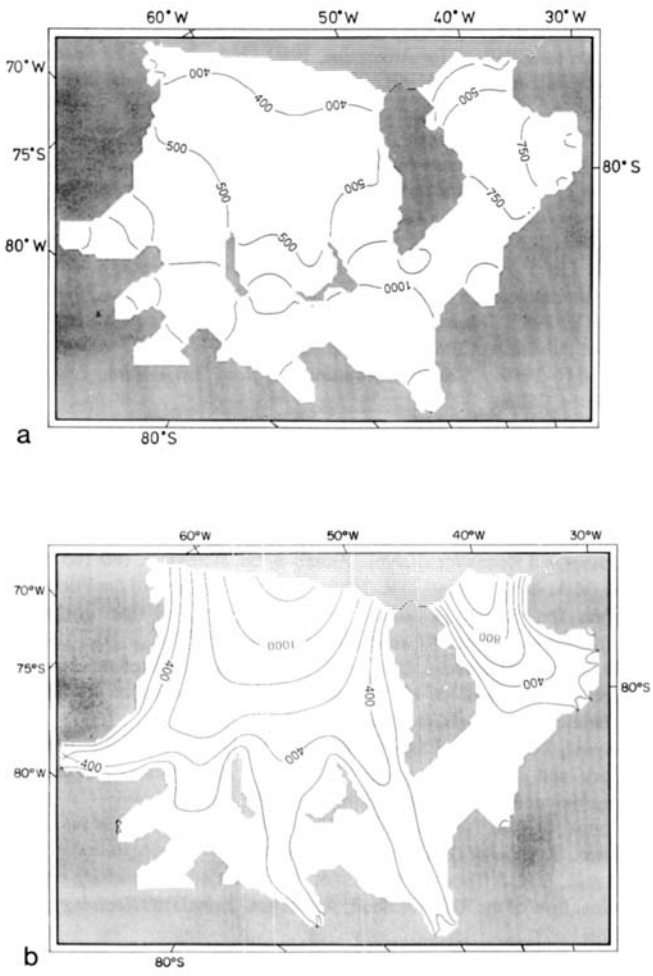

Fig. 6. **a)** Run B: ice thickness distribution after 2000 years of future evolution; surface accumulation only. The shape of the ice shelf has changed markedly. Downstream of Henry and Korff the ice shelf has thinned while at the ice front thicknesses have increased by up to 200 m. Two thin regions in the western part have disappeared.
b) Run B - correspondent velocity field after 2000 a. Velocities at the ice front have decreased by up to 300 m a^{-1}. Due to increased thicknesses at the grounding line ice streams now propagate more strongly into the ice shelf.

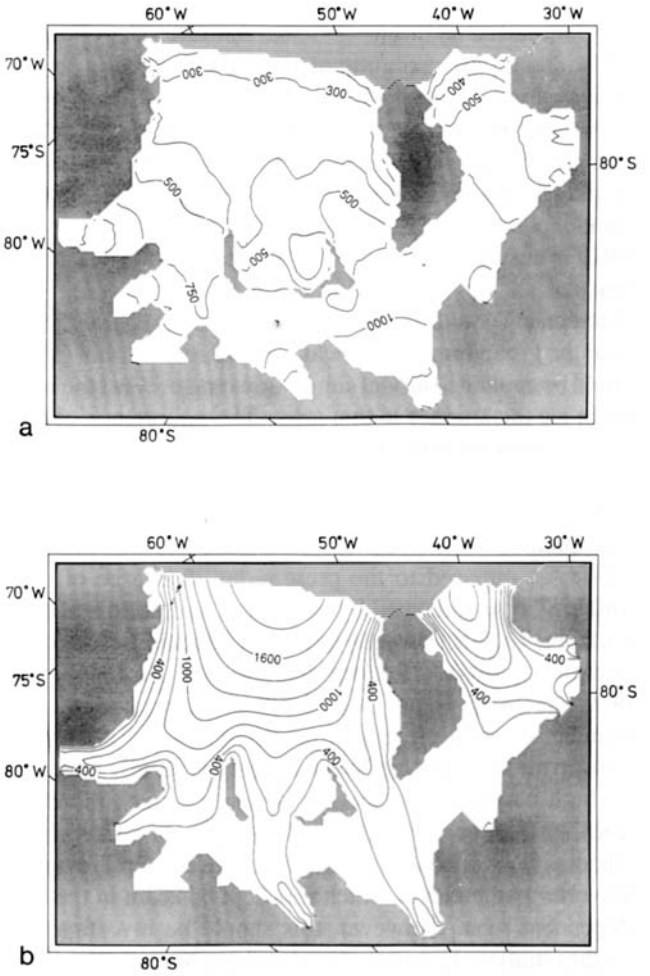

Fig. 7.a) Run C: ice thickness distribution after 2000 years of future evolution . Regions where melting and freezing have occurred, showing altered ice thicknesses. Downstream of Henry and Korff ice rises the thin region has disappeared, while melting has caused a remarkable thinning at the ice front.
b) Run C: correspondent velocity field after 2000 years of future evolution. Compared with run B, velocities at the ice front are different. At the Ronne side they are about 200 m a^{-1} higher.

propagate more strongly into the ice shelf, whereas the ice front velocities decrease, especially for Filchner, where a reduction of up to 300 m a^{-1} is recorded.

Figs. 7a & b express the results of run C, which takes into account bottom melting and accumulation. Thicknesses at the grounding line are similar to those in run B, whereas areas of basal melting reach a new steady state. In the central area, a dome-like shape has evolved, while at the ice front thicknesses approach almost present-day conditions. Velocity magnitudes at the ice front slightly exceed present values; on approaching the grounding line they equal those of run B.

Although a downstream-increasing ice thickness is not very likely, it is consistent with the model constraints. Because of high bottom accretion rates, a new shape evolves which implies a new velocity field. Thereby, a balance of accumulation and thinning as a result of spreading holds at the end of a simulation.

Conclusions

The model used is clearly a good tool to investigate ice shelf dynamics. Although neglecting lateral temperature variations might imply velocity deviations locally, the overall results are convincing. Of course, a more accurate definition of model boundaries and temperatures would improve the results further but this would require extensive future field

https://doi.org/10.1017/S0954102091000226 Published online by Cambridge University Press

programmes in addition.

The small grid resolution of 10 x 10 km allows a detailed investigation of local effects, such as basal melting and freezing or small-scale flow across ice rumples. Addressing the mass budget of ice shelves, it is essential to discuss the processes that occur at the ice shelf bottom. Although the time-dependent simulations suggest that the present state of FRIS is unstable, I favour Van der Veen's (1986) statement that ice shelves are always close to steady state. This discrepancy could be dismissed if substantial basal melting near the grounding line, as was postulated by Robin (1979), could be applied to model simulations and prevent the build-up in ice thicknesses in that area. The importance of basal melting may become clear from some quantities related to FRIS. Following McIntyre (1986), the total influx from ice streams equals 235 $km^3 a^{-1}$. Together with an annual precipitation of 91 $km^3 a^{-1}$, there is more than 320 $km^3 a^{-1}$ of influx, as opposed to the present-day discharge of about 180 $km^3 a^{-1}$ as indicated by horizontal advection across the ice front. This fact strongly implies substantial basal melting underneath FRIS. Bottom accretion in the central part, downstream of Henry and Korff ice rises, increases the volume of melting which is necessary to obey mass conservation. Although basal melting is locally restricted, its high magnitude affects ice dynamics much more than does surface accumulation. According to MacAyeal & Thomas (1986), basal melting influences the depth-averaged flow law parameter A which was kept constant in the time-dependent runs. However, this should be investigated in further studies. Extensive basal melting not only affects the steady state profile of FRIS, but also creates an important heat sink in the submerging ocean.

Acknowledgements

I would like to thank J. Oerlemans for initial supervision, P. Huybrechts for helpful comments and M. Lange for providing ice thickness data. I also thank two anonymous reviewers for their critical remarks on the manuscript which was carefully edited by M.J. Hambrey. This is contribution No. 351 of the Alfred Wegener Institute for Polar and Marine Research.

References

Behrendt, J.C. 1970. The structure of the Filchner Ice Shelf and its relation to bottom melting. *In* Gow, A.J., Keller, C., Langway, C.C. & Weeks, W. F. *eds. International Symposium on Antarctic Glaciological Exploration (ISAGE)*, Hannover, N.H., September 3-7, 1968, IASH Publication No 86, 488-496.

Bindschadler, R. 1983. The importance of pressurized subglacial water in separation and sliding at the glacier bed. *Journal of Glaciology*, **29**, 3-19.

Budd, W.F. 1966. The dynamics of the Amery Ice Shelf. *Journal of Glaciology*, **6**, 335-358.

Budd, W.F., Keage, P.L. & Blundy, N.A. 1979. Empirical studies of ice sliding. *Journal of Glaciology*, **23**, 157-170.

Englehardt, H. & Determanm. J. 1987. Borehole evidence for a thick layer of basal ice in the central Ronne Ice Shelf. *Nature*, **327**, 318-319.

Giovinetto, M.B. & Bull, C. 1987. Summary and analyses of surface mass balance compilations for Antarctica, 1960-1985. *Byrd Polar Research Center Report No. 1*, 61-68. Columbus: Ohio, Byrd Polar Research Center.

Glen, J.W. 1955. The creep of polycrystalline ice. *Proceedings of the Royal Society of London* Series A, **228**, 519-538.

Heterich, K. 1987. On the flow within the transition zone of an ice sheet and ice shelf. *In* Veen, C.J. Van der, & Oerlemans, *eds. Dynamics of the West Antarctic Ice Sheet*. Dordrecht: D. Reidel Publishing Company, 185-202.

Holton, J.R. 1979. *An Introduction to Dynamic Meteorology*. Vol. 23. *International Geophysics Series*. New York: Academic Press, 391pp.

Hutter, K. 1983. *Theoretical Glaciology*, Hingham, Massachusetts: De Reidel Publishing Company, 510pp.

Jaeger, J.C. 1969. *Elasticity, fracture and flow*, 3rd Edition, London: Methuen, 268pp.

Kock, H. & Wiegand, A. 1986. Glaciological geodesy on Filchner Ice Shelf 1983-86. *In* Kohnen, H. *comp. Filchner-Ronne-Ice Shelf Programme. Report No. 3*. Bremerhaven: Alfred Wegener Institute for Polar and Marine Research, 37-42.

Kohnen, H. 1982. Glaciological investigations in the frontal zone of the Filchner and Ronne ice shelves. *Annals of Glaciology*, **3**, 160-165.

Lange, M.A. & MacAyeal, D.R. 1986. Numerical models of the Filchner-Ronne Ice Shelf: an assessment of reinterpreted ice thickness distributions. *Journal of Geophysical Research, 91* (B10), 10457-10462.

Lange, M.A. & MacAyeal, D.R. 1988. Numerical models of steady-state thickness and basal ice configuration of the central Ronne Ice Shelf, Antarctica. *Annals of Glaciology*, **11**, 64-70.

MacAyeal, D.R. 1989. Large-scale flow over a viscous basal sediment: theory and application to Ice Stream B, Antarctica. *Journal of Geophysical Research*, **94** (B4), 4071-4087.

MacAyeal, D.R. & Thomas, R.H. 1982. Numerical modelling of ice shelf motion. *Journal of Glaciology*, **3**, 189-194.

MacAyeal, D.R. & Thomas, R.H. 1986. The effect of basal melting on the present flow of the Ross Ice Shelf, Antarctica. *Annals of Glaciology*, **32**, 72-86

McIntyre, N.F. 1986. Discharge of ice into the Filchner-Ronne ice shelves. *In* Kohnen, H. *comp. Filchner-Ronne-Ice Shelf Programme. Report No. 3*. Bremerhaven: Alfred Wegener Institute for Polar and Marine Research, 47-52.

Muszinski, I & Birchfield, G.E. 1987. A coupled marine ice stream-ice shelf model. *Journal of Glaciology*, **33**(113), 3-15.

Paterson, W.S.B. 1981. *The Physics of glaciers*, 2nd Edition. Oxford: Pergamon Press, 380pp.

Robin, G. de Q. 1979. Formation, flow and disintegration of floating ice shelves. *Journal of Glaciology*, **24**, 259-271.

Sanderson, T.J.O. 1979. Equilibrium profiles of ice shelves. *Journal of Glaciology*, **22**, 435-460.

Sanderson. T.J.O. & Doake, C.S.M. 1979. Is vertical shear in an ice shelf negligible? *Journal of Glaciology*, **22**(87), 285-292.

Smith, A.M. 1986. Ice rumples between Korff and Henry ice rises. *In*, Kohnen, H. *comp. Filchner-Ronne-Ice Shelf Programme. Report No. 3*. Bremerhaven, Alfred Wegener Institute for Polar and Marine Research, 81-83.

Swithinbank, C. 1986. Ice rises and rumples. *In* Kohnen, H. *comp. Filchner-Ronne-Ice Shelf Programme. Report No. 3*. Bremerhaven: Alfred Wegener Institute for Polar and Marine Research, 11-14.

Swithinbank, C. 1988. Satellite image atlas of the glaciers of the world. *US Geological Survey Professional Paper*, No. 1386-B.

Thomas, R.H. 1973. The creep of ice shelves: theory. *Journal of Glaciology*, **12**, 45-53.

Thyssen, F. 1988. Special aspects of the central part of the Filchner-Ronne Ice Shelf, Antarctica. *Annals of Glaciology*, **11**, 173-179.

Van der Veen, J.C. 1986. Numerical modelling of ice shelves and ice tongues. *Annales Geophysicae*, **4**(B1), 45-54.

Weeterman, J. 1957. Deformation of floating ice shelves. *Journal of Glaciology*, **3**, 38-42.

Appendix

Numerical procedure

The set of equations (19) together with the boundary conditions of mixed type can be solved numerically by means of a successive relaxation scheme (Holton 1979). This is done iteratively on a 10 x 10 km grid, starting with u=v=0 everywhere except at the grounding line, where ice streams determine velocity magnitudes locally. All first and second order derivatives can be centred in space and then be expressed in a finite difference form as:

$$\begin{aligned}
&\tfrac{2}{5}\Big(u(i+1,j)_{k-1}+u(i-1,j)_k\Big)\\
&+\tfrac{1}{10}\Big(u(i,j-1)_{k-1}+u(i,j+1)_{k-1}\Big)\\
&+\tfrac{3}{40}\Big(v(i+1,j+1)_{k-1}+v(i-1,j-1)_k\\
&-v(i-1,j+1)_k-v(i+1,j-1)_{k-1}\Big)\\
&-\tfrac{1}{20}\Delta x\Big(z_s(i+1,j)-z_s(i-1,j)\Big)f(i,j)_k\gamma(i,j)\\
&-u(i,j)_{k-1}=0 \qquad (A1)
\end{aligned}$$

and respectively:

$$\begin{aligned}
&\tfrac{2}{5}\Big(v(i,j+1)_{k-1}+v(i,j-1)_k\Big)\\
&+\tfrac{1}{10}\Big(v(i-1,j)_{k-1}+v(i+1,j)_{k-1}\Big)\\
&+\tfrac{3}{40}\Big(u(i+1,j+1)_{k-1}+u(i-1,j-1)_k\\
&-u(i-1,j+1)_k-u(i+1,j-1)_{k-1}\Big)\\
&-\tfrac{1}{20}\Delta y\Big(z_s(i,j+1)-z_s(i,j-1)\Big)f(i,j)_k\gamma(i,j)\\
&-v(i,j)_{k-1}=0 \qquad (A2)
\end{aligned}$$

where

$$\begin{aligned}
f(i,j)_k=&\Big[\Big(\frac{u(i+1,j)_{k-1}-u(i-1,j)_{k-1}}{2\Delta x}\Big)^2\\
&+\Big(\frac{v(i,j+1)_{k-1}-v(i,j-1)_{k-1}}{2\Delta x}\Big)^2\\
&+\Big(\frac{u(i+1,j)_{k-1}-u(i-1,j)_{k-1}}{2\Delta x}\Big)\\
&\times\Big(\frac{v(i,j+1)_{k-1}-v(i,j-1)_{k-1}}{2\Delta x}\Big)\\
&+\frac{1}{4}\Big(\frac{u(i,j+1)_{k-1}-u(i,j-1)_{k-1}}{2\Delta x}\\
&+\frac{v(i+1,j)_{k-1}-v(i-1,j)_{k-1}}{2\Delta x}\Big)^2\Big]^{-\frac{1-n}{2n}} \qquad (A3)
\end{aligned}$$

and

$$\gamma(i,j)=\rho_i(i,j)gA^{\frac{1}{3}}. \qquad (A4)$$

Equations (A.1) and (A.2) are solved for u(i,j) and v(i,j) which are the velocity components at the central grid point. f(i,j)$_k$ is defined using velocities from the previous guess (k-1). In order to save computation time, the terms $\partial f/\partial x$ and $\partial f/\partial y$ have been neglected in the development of the numerical solution. They were found to be of minor importance to the solution. After about 5000 iterations, the solution is within 5–10% of asymptotic state which can be estimated from the increase of kinetic energy inherent to the system (Fig. 8).

Now, having derived the velocity field for a given ice thickness distribution, transient changes of the ice shelf shape are investigated using the mass conservation equation (24). In terms of centred differences, the new ice thickness at time $t+dt$ at node (i,j) arises from:

$$\begin{aligned}
&H(i,j)^{t+\Delta t}=H(i,j)^t\\
&-\Big[\frac{H(i+1,j)u(i+1,j)}{2\Delta x}-\frac{H(i-1,j)u(i-1,j)}{2\Delta x}\Big]^t\\
&-\Big[\frac{H(i,j+1)u(i,j+1)}{2\Delta x}-\frac{H(i,j-1)u(i,j-1)}{2\Delta x}\Big]^t\\
&+a(i,j)-m(i,j). \qquad (A5)
\end{aligned}$$

In a time-dependent simulation, ice thickness changes are small and thus only few iterations are needed to re-evaluate the velocity field. A time step of 0.5 a was found to provide a good progress in the prognostic runs, which are extended to 2000 a of future ice shelf evolution.

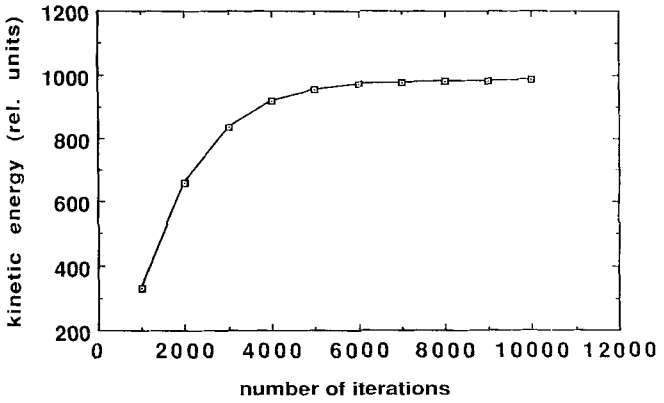

Fig. 8. Convergence of the solution: kinetic energy in the system versus number of iterations

https://doi.org/10.1017/S0954102091000226 Published online by Cambridge University Press